Supplementary Information for

Zinc Complex Based Multifunctional Reactive Lithium Polysulfide Trapper Approaching Its Theoretical Efficiency

Zhong Ma[1, †], Zhijun Zuo[2, †], Yuning Li[1,*]

[1]Department of Chemical Engineering and Waterloo Institute for Nanotechnology (WIN), University of Waterloo, Waterloo, Ontario N2L 3G1, Canada

[2]Key Laboratory of Coal Science and Technology of Ministry of Education and Shanxi Province, Taiyuan University of Technology, Taiyuan, Shanxi 030024, China

[†]These authors contributed equally to this work

*Corresponding author. E-mail: yuning.li@uwaterloo.ca

1. Supplementary Materials and Methods

Definitions of molecular (or molar) efficiency (η_n) and mass efficiency (η_m) for LPS trappers

The molecular (or molar) efficiency (η_n) for a LPS trapper is defined as the number of LPS molecules trapped by one trapper molecule or moles of LPS trapped by one mole of trapper molecules as shown in Eq. (1):

$$\eta_n = \frac{n_{\mathrm{LPS}}}{n_{\mathrm{trap}}} = \frac{\frac{m_{LPS}}{M_{LPS}}}{\frac{m_{trap}}{M_{trap}}} \left(\frac{mol_{LPS}}{mol_{trap}}\right) \quad (1)$$

where n_{LPS}, m_{LPS}, and M_{LPS} are the number of moles, mass (g), and molar mass (g mol^{-1}) of soluble LPS, respectively, while n_{trap}, m_{trap}, M_{trap} are the number of moles, mass (g), and molar mass (g mol^{-1}) of the trapper, respectively. For an inorganic compound, e. g., MoS_2, the molar mass of the compound formula (160.07 g mol^{-1} for MoS_2) is used as M_{trap}. If a polymer is used as the LPS trapper, the molar mass of the repeat unit, instead of the actual molecular weight of the polymer, is used as M_{trap}.

The mass efficiency for LPS trapping, η_m, is defined as the mass (g) of soluble LPS being trapped by per gram of LPS trapper shown in Eq. (2), which is equivalent to the adsorption capacity used in ref. 1.

$$\eta_m = \frac{m_{\mathrm{LPS}}}{m_{\mathrm{trap}}} \left(\frac{g_{LPS}}{g_{trap}}\right) \quad (2)$$

where m_{LPS} and m_{trap} are defined as above.

The conversion between η_n and η_m is shown in Eq. (3):

$$\eta_n = \eta_m \times \frac{M_{trap}}{M_{LPS}} \quad (3)$$

where M_{LPS} and M_{trap} are defined as above.

Model reactions for first-principles density functional calculations

The reduction reactions of S_8 and LPS[2] and corresponding zinc complexes are proposed as follows, which are used for calculating the Gibbs free energy changes (ΔG).:

ΔG_1: $2Li+S_8^* \rightarrow Li_2S_8^*$

$Zn(OAc)_2 \cdot DEA^* + 2S_8^* + 4Li \rightarrow Zn(S_8Li)_2 \cdot DEA^* + 2^* + 2LiOAc$

ΔG_2: $3Li_2S_8^* + 2Li + ^* \rightarrow 4Li_2S_6^*$

$Zn(S_8Li)_2 \cdot DEA^* + 4Li + 2^* \rightarrow Zn(S_6Li)_2 \cdot DEA^* + 2Li_2S_2^*$

ΔG_3: $2Li_2S_6^* + 2Li + ^* \rightarrow 3Li_2S_4^*$

$Zn(S_6Li)_2 \cdot DEA^* + 4Li + 2^* \rightarrow Zn(S_4Li)_2 \cdot DEA^* + 2Li_2S_2^*$

ΔG_4: $Li_2S_4^* + 2Li + ^* \rightarrow 2Li_2S_2^*$

$Zn(S_4Li)_2 \cdot DEA^* + 4Li + 2^* \rightarrow Zn(S_2Li)_2 \cdot DEA^* + 2Li_2S_2^*$

ΔG_5: $Li_2S_2^* + 2Li + ^* \rightarrow 2Li_2S^*$

$Zn(S_2Li)_2 \cdot DEA^* + 4Li + ^* \rightarrow Zn(SLi)_2 \cdot DEA^* + 2Li_2S^*$

where * represents a graphene substrate.

2. Legends for movies S1-S4

87 μmol of zinc acetate and 87 μmol of DEA were dissolved in 3 mL CD_3OD to form a solution, which was divided into three portions. Two of these samples was added by the desired amount of Li_2S_6 with 1 or 2 times molar ratios.

Movie S1: The reaction between Li_2S_6 and $Zn(OAc)_2$·DEA in CD_3OD with a molar ratio of 1:1.

This movie clip shows a clear colorless $Zn(OAc)_2$·DEA solution in CD_3OD turned turbid with formation of white precipitates when adding 1 eq. of Li_2S_6 in DME/DOL (*v:v*=1:1).

Movie S2: The reaction between Li_2S_6 and $Zn(OAc)_2$·DEA in CD_3OD with a molar ratio of 2:1.

This movie clip shows a clear, colorless $Zn(OAc)_2$·DEA solution in CD_3OD first turned turbid with formation of white precipitates, then changed into a clear, yellow solution when gradually adding 2 eq. of Li_2S_6 in DME/DOL (*v:v*=1:1).

Movie S3: The reaction between Li_2S and $Zn(OAc)_2$·DEA in CD_3OD with a molar ratio of 2:1.

This movie clip shows a clear, colorless $Zn(OAc)_2$·DEA solution in CD_3OD turned turbid with formation of white precipitates when adding 2 eq. of Li_2S in CD_3OD.

Movie S4: The reaction between Li_2S_6 and the products of Li_2S and $Zn(OAc)_2$·DEA in CD_3OD made in Movie S3 with a molar ratio of 2:1.

This movie clip shows the turbid solution of Li_2S and $Zn(OAc)_2$·DEA made in Movie S3 gradually changed into a brightly yellow solution when adding 2 eq. of Li_2S_6 in DME/DOL (*v:v*=1:1). The white precipitates disappeared completely in the end.

3. Supplementary Figures

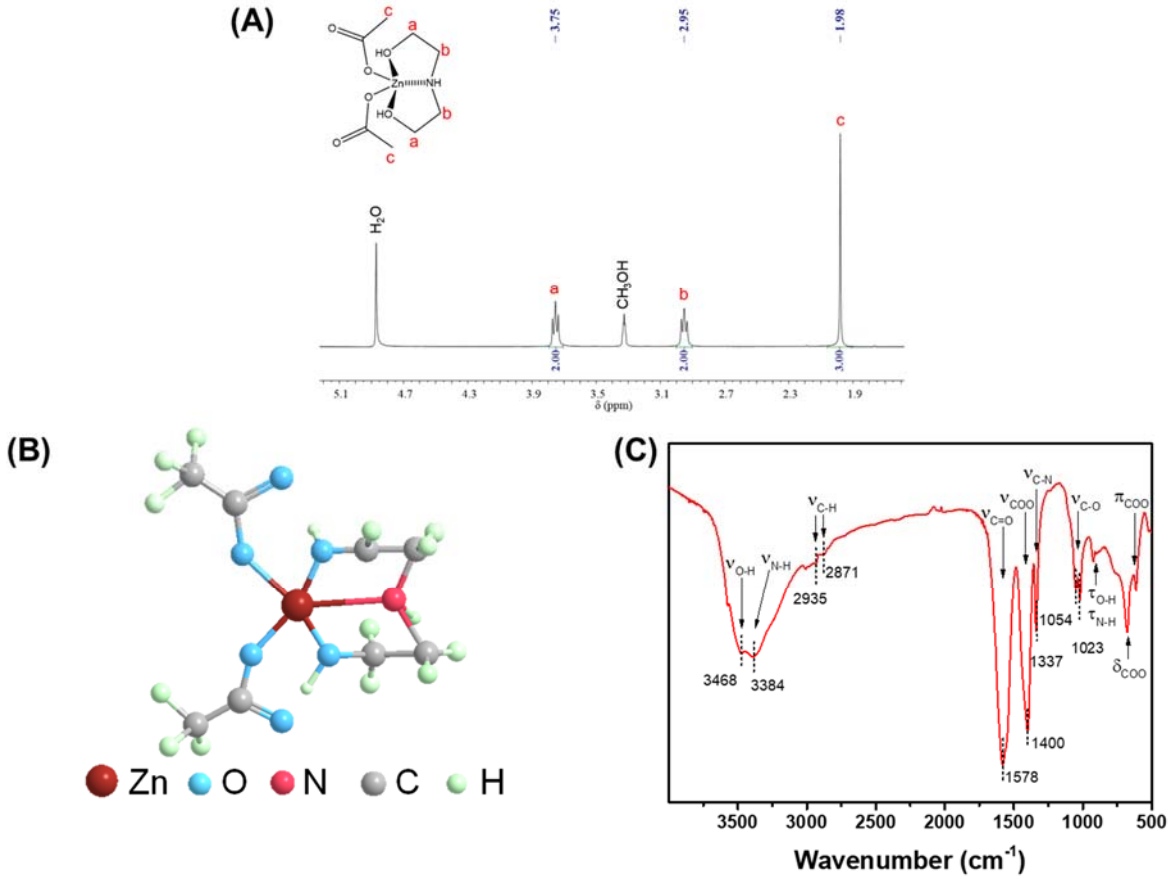

Fig. S1 (A) ^{1}H NMR spectrum of $Zn(OAc)_2 \cdot DEA$ in CD_3OD. The sample for the NMR measurement was obtained by freeze-drying an aliquot of the Zn-DEA solution in ethanol. ^{1}H NMR, 300 MHz, CD_3OD: δ=1.98 (s, 6H, CH_3), 2.95 (t, *J*= 5.0 Hz, 4H, CH_2-N), 3.75 (t, *J*=5.0 Hz, 4H, O-CH_2) ppm, which agree with the data reported in the literature[3]. **(B)** The 3-D structure comprising four $Zn(OAc)_2 \cdot DEA$ molecules drawn using the single crystal XRD data published in the literature *(28)*. Dashed lines represent hydrogen bonds. **(C)** Fourier-transform infrared (FT-IR) spectroscopy of $Zn(OAc)_2 \cdot DEA$. The wavenumbers of 3468, 3384, 2935, 2871, 1578, 1400, 1337, 1054, 1023, 918, 673, and 613 cm^{-1} correspond to the stretching vibrations of O-H, N-H, C-H, C=O, COO, C-O, respectively, which agree with the data reported in the literatures[3,4].

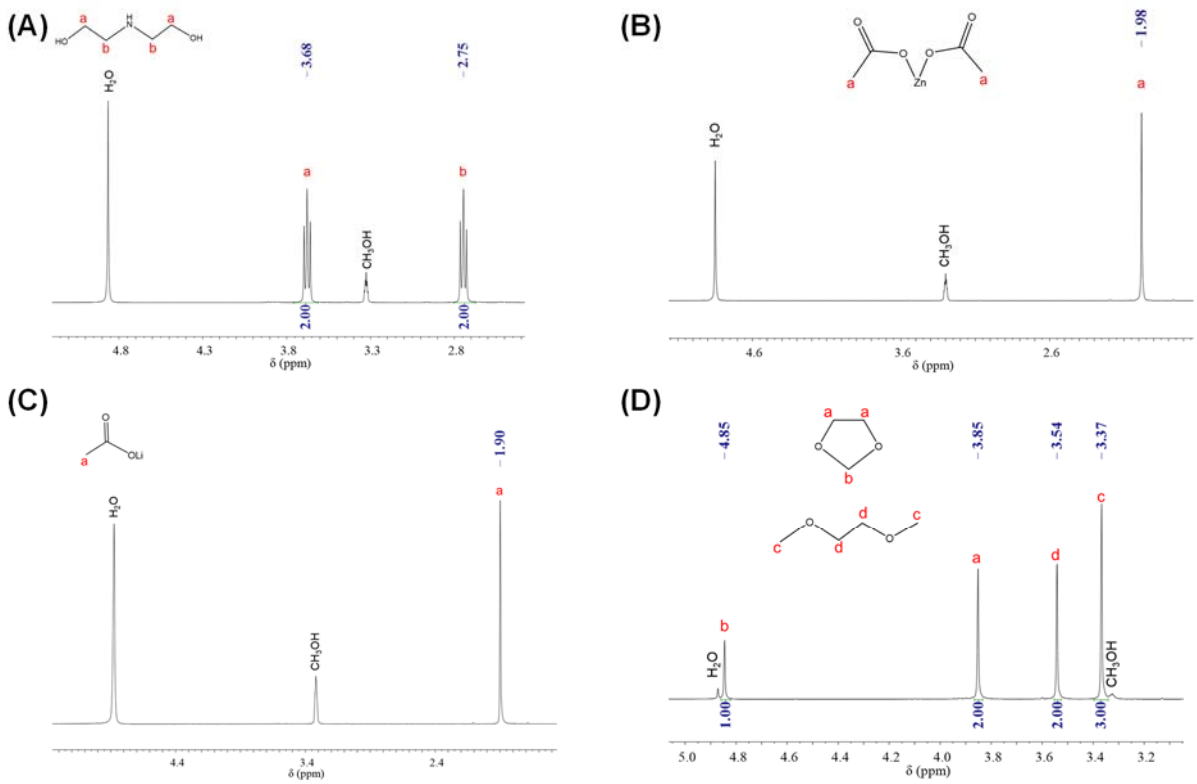

Fig. S2 ^{1}H NMR spectrum of **(A)** DEA, **(B)** zinc acetate, **(C)** lithium acetate and **(D)** Li_2S_6 with DME/DOL in CD_3OD.

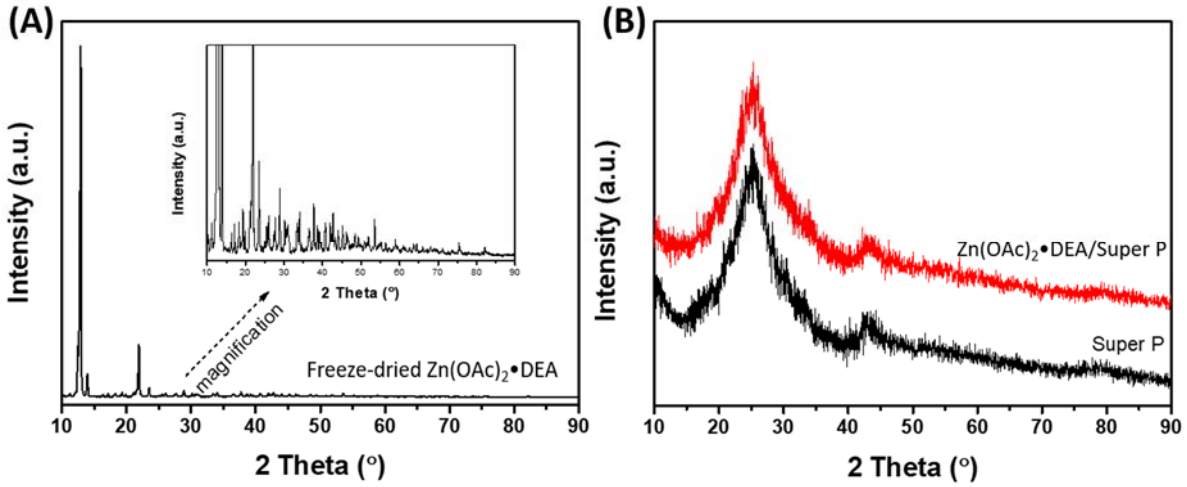

Fig. S3 XRD patterns of **(A)** freeze-dried $Zn(OAc)_2 \cdot DEA$ and **(B)** Super P and $Zn(OAc)_2 \cdot DEA$/Super P mixture with a mass ratio of 1:3.6, which was prepared by sonicating a mixture of Super P and $Zn(OAc)_2 \cdot DEA$ in ethanol, followed by drying at 50 ℃.

The XRD pattern of freeze-dried $Zn(OAc)_2 \cdot DEA$ shows distinct diffraction peaks, indicating its high crystallinity, while XRD pattern of the Zn-DEA/Super P mixture shows no obvious diffraction peaks associated to $Zn(OAc)_2 \cdot DEA$, indicating that $Zn(OAc)_2 \cdot DEA$ was homogeneously dispersed in the mixture.

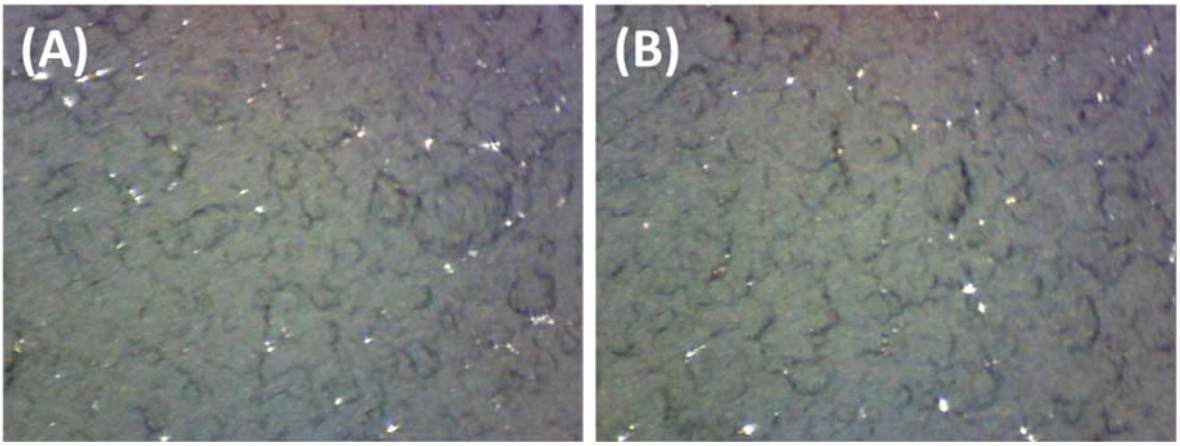

Fig. S4 The optical microscopic images of the sulfur electrodes on carbon-coated Al substrates prepared using **(A)** $Zn(OAc)_2 \cdot DEA$ and **(B)** PVDF as binder, respectively.

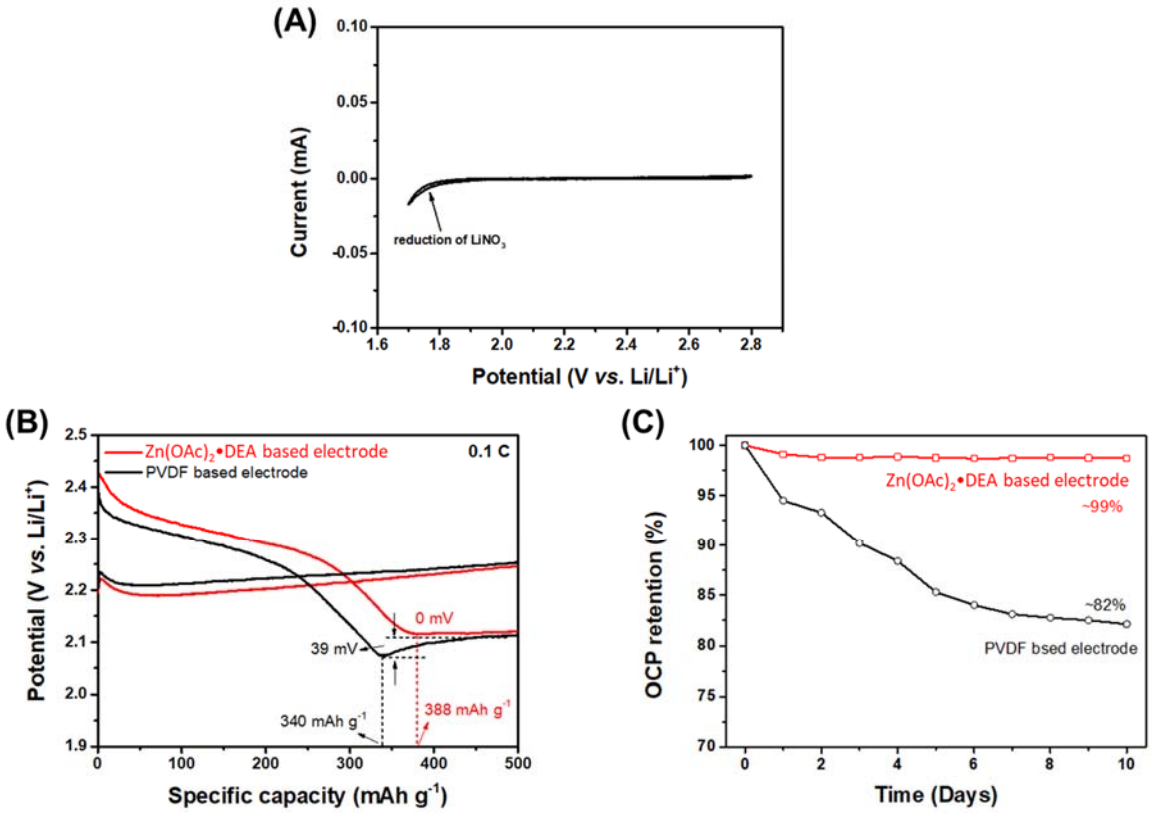

Fig. S5 (A) CV curve of $Zn(OAc)_2$·DEA based electrode. The $Zn(OAc)_2$·DEA electrode was prepared by coating a slurry containing Zn-DEA and Super P with a mass ratio of 1:1 and was tested at a scan rate of 0.1 mV s^{-1} in the potential range of 1.7 -2.8 V. No obvious peaks associated to the reaction of $Zn(OAc)_2$·DEA were detected in this potential range, indicating the good stability of $Zn(OAc)_2$·DEA during the LSBs discharge-charge process. **(B)** Partial charge/discharge curves of Zn-DEA and PVDF based electrodes at 0.1 C in the first cycle. **(C)** Self-discharge behaviors of LSBs with $Zn(OAc)_2$·DEA or PVDF as binder by monitoring the open circuit potentials of the batteries over a period of 10 days.

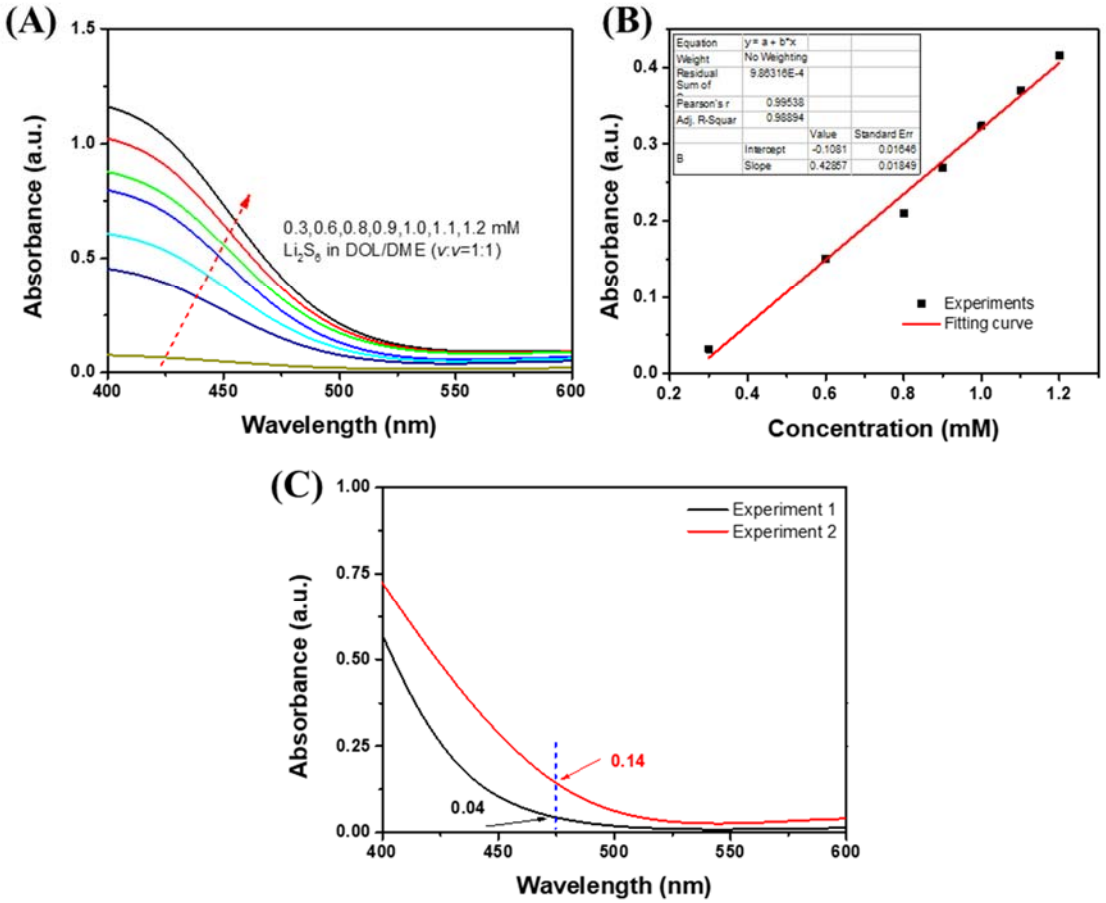

Fig. S6 LPS (Li_2S_6 was used as a representative of LPS) trapping tests with $Zn(OAc)_2$·DEA using UV-vis spectroscopy. **(A)** UV-Vis curves of Li_2S_6 solutions in DOL/DME with varying concentrations. **(B)** Calibration curve of absorbance (taken at 475 nm) versus concentration of Li_2S_6 obtained from (A), which has a linear fitting shown in Eq. (4):

$$A = 0.4285c - 0.1081 \quad (4)$$

where A is the absorbance and c is the concentration (with the unit of mM) of the sample. **(C)** UV-Vis curves of the supernatant solutions of $Zn(OAc)_2$·DEA/Super P with excess Li_2S_6 in DOL/DME with details described in Experiment 1 and Experiment 2 as follows.

LPS trapping: $Zn(OAc)_2$·DEA, Super P and Li_2S_6 were mixed in 4 ml DOL/DME for 3 h and the mixture was diluted 10 times with DOL/DME. The supernatant was subjected to the UV

measurement. Two experiments were carried out. The experimental details and results are shown in Fig. S6C and Table S1.

The LPS trapping efficiencies of $Zn(OAc)_2$·DEA were calculated as follows.

The LPS concentrations of the two samples from the two experiments, c_1 and c_2, were calculated using their UV-vis absorbance values shown in Fig. S6C according to Eq. (4),

$$c_1 = \frac{A_1+0.1081}{0.4285} = \frac{0.04+0.1081}{0.4285} = 0.346 \text{ mM} \quad (5)$$

$$c_2 = \frac{A_2+0.1081}{0.4285} = \frac{0.14+0.1081}{0.4285} = 0.579 \text{ mM} \quad (6)$$

The molecular efficiency η_n of $Zn(OAc)_2$·DEA for LPS trapping can be calculated using Eq. (7)

$$\eta_n = \frac{c_o - c}{c_{Zn-DEA}} \quad (7)$$

where c_o and c are the concentrations of Li_2S_6 in the diluted solution before (original) and after (actual concentration in the supernatant determined by UV-vis) trapping occurs, respectively, while c_{Zn-DEA} is the original concentration of $Zn(OAc)_2$·DEA in the diluted solution.

Based on the Eq. (7), the molecular efficiencies of $Zn(OAc)_2$·DEA for LPS trapping in Experiments 1 and 2 were calculated as follows:

$$\eta_{n1} = \frac{c_{o1}-c_1}{c_{Zn-DEA1}} = \frac{1.25-0.346}{0.52} = 1.74 \quad (8)$$

$$\eta_{n2} = \frac{c_{o2}-c_2}{c_{Zn-DEA2}} = \frac{0.938-0.579}{0.195} = 1.84 \quad (9)$$

Finally, the average η_n of $Zn(OAc)_2$·DEA:

$$\eta_n = \frac{\eta_{n1}+\eta_{n2}}{2} = \frac{1.74+1.84}{2} \cong 1.8 \left(\frac{\text{mol}_{LPS}}{\text{mol}_{Zn-DEA}}\right)$$

The mass efficiency η_m is calculated using Eq. (3):

$$\eta_m = \eta_n \times \frac{M_{LPS}}{M_{Zn-DEA}} = 1.8 \times \frac{206.24 g/mol}{288.61 g/mol} \cong 1.3 \left(\frac{g_{LPS}}{g_{Zn-DEA}}\right)$$

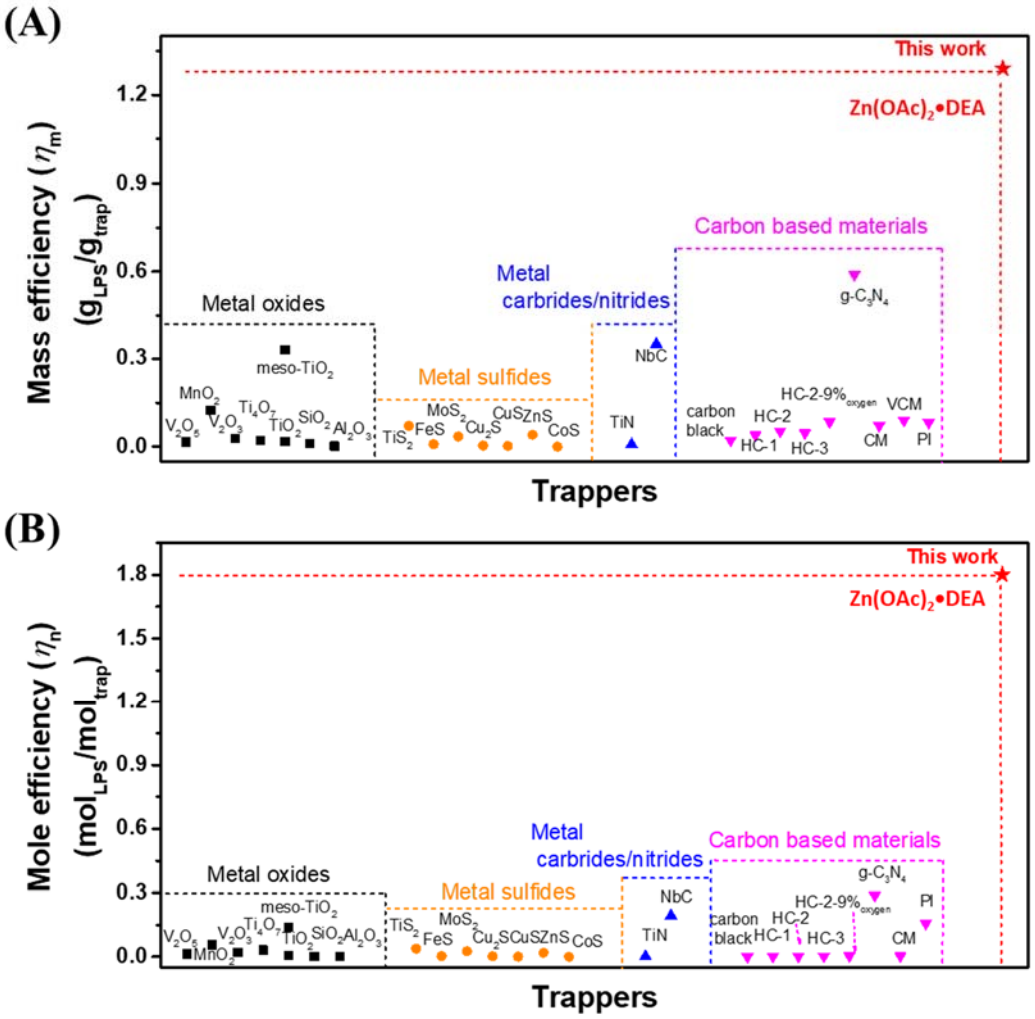

Fig. S7 LPS trapping capability of $Zn(OAc)_2$·DEA in **(A)** mass efficiency and **(B)** mole efficiency in comparison with some reported LPS trappers in the literature. (Data and references are listed in Table S2)

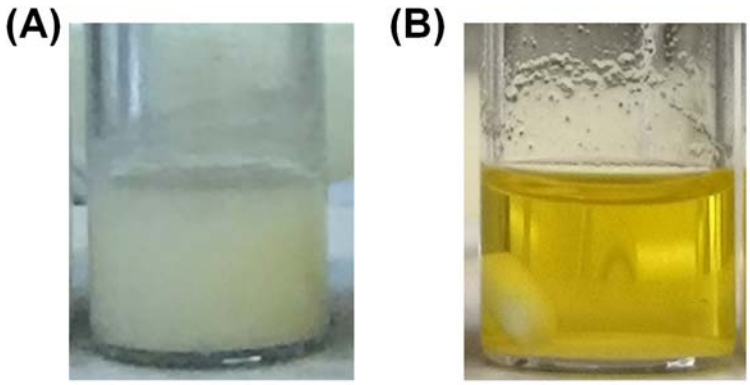

Fig. S8 Digital photos of the as-prepared solution of Li_2S_6 and $Zn(OAc)_2$·DEA with a molar ratio of **(A)** 1:1 and **(B)** 2:1 in CD_3OD.

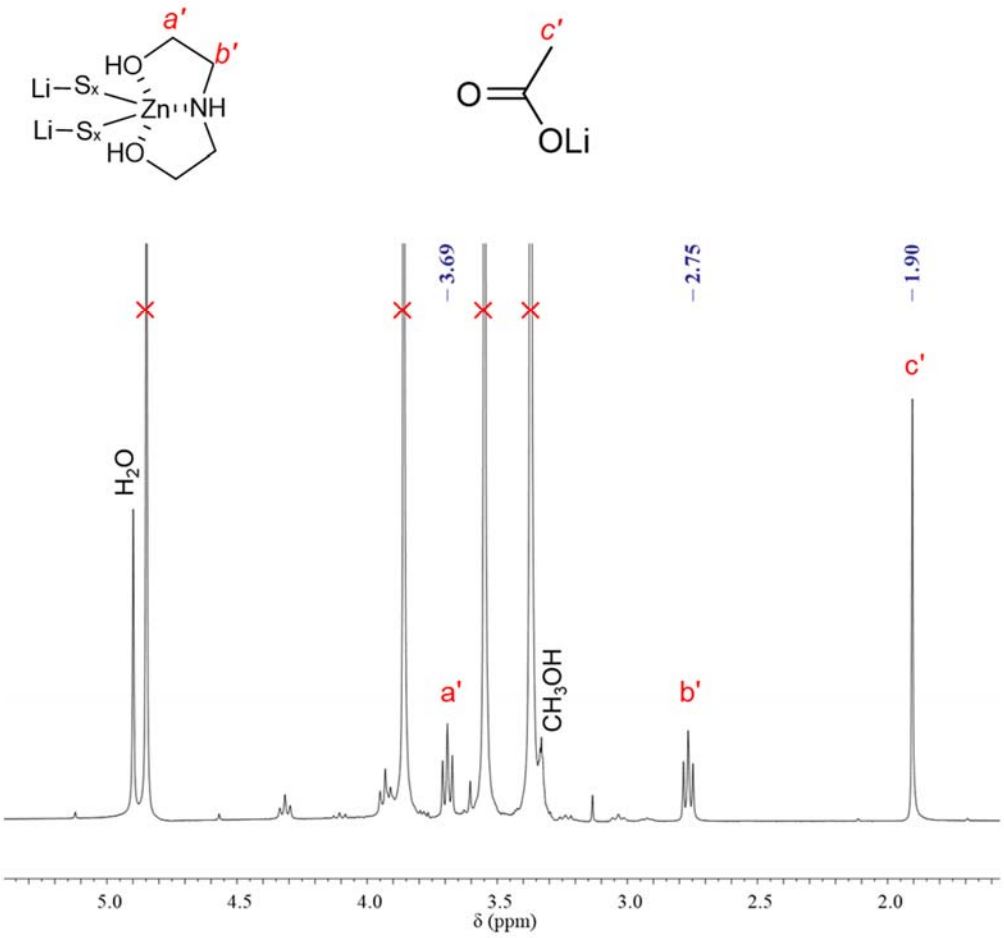

Fig. S9 ^{1}H NMR spectrum of $Zn(OAc)_2 \cdot DEA$ in CD_3OD with the addition of 7 eq. of Li_2S_6.

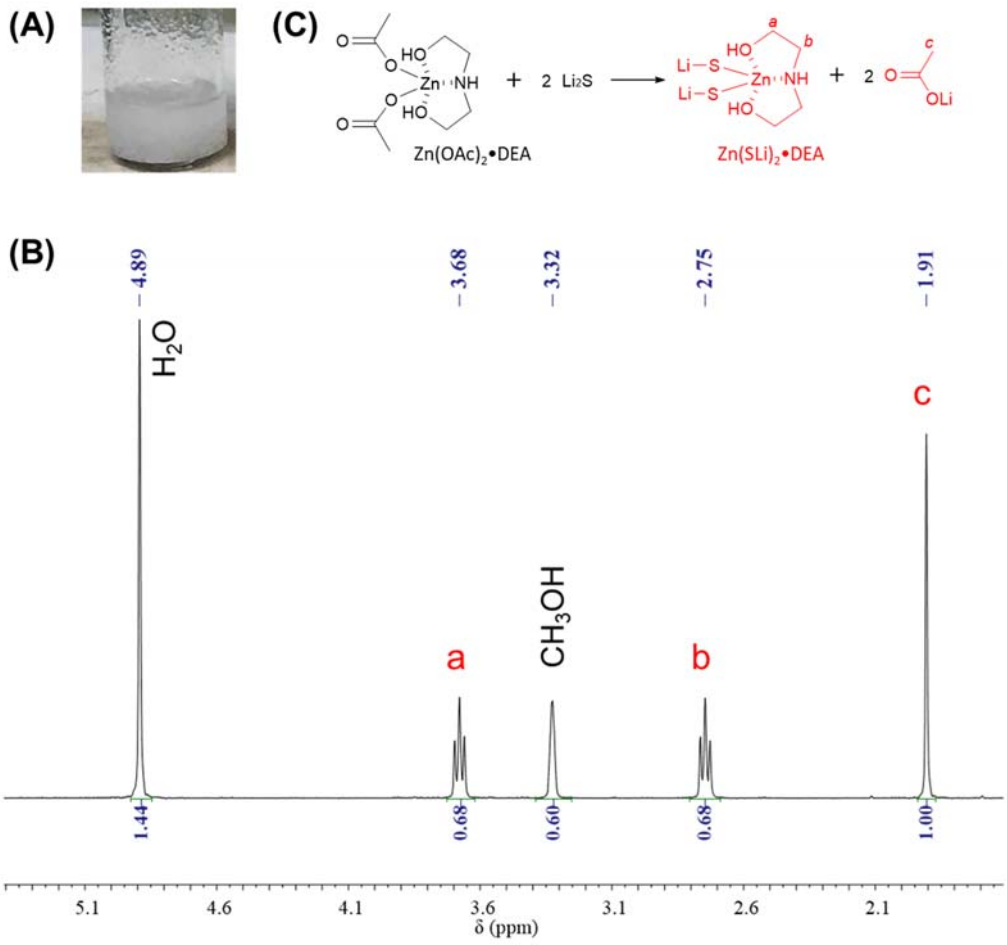

Fig. S10 (A) Digital photo and **(B)** ^{1}H NMR spectrum of the as-prepared solution of Li_2S and $Zn(OAc)_2$·DEA with molar ratio of 2:1 in CD_3OD; **(C)** The proposed reaction between $Zn(OAc)_2$·DEA and Li_2S.

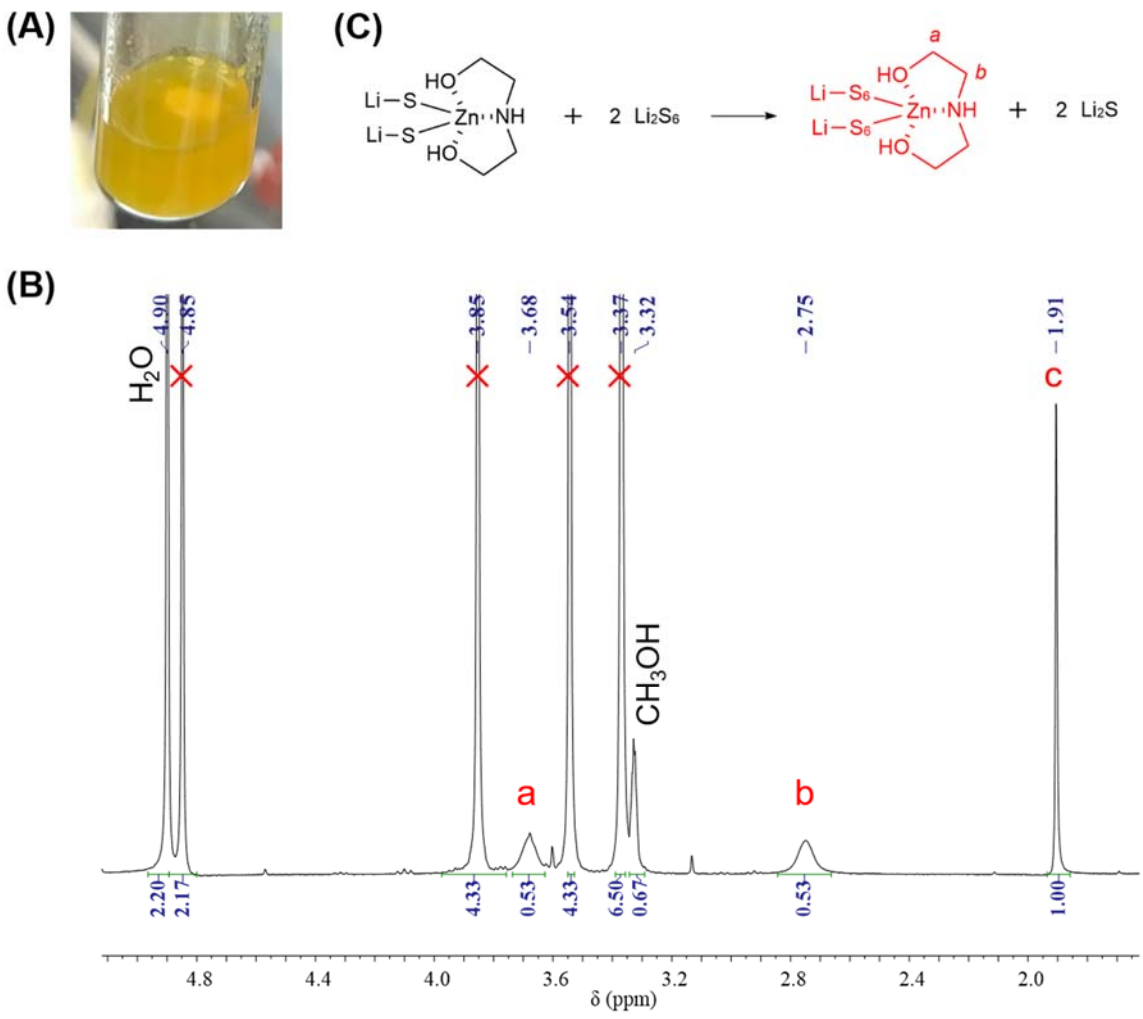

Fig. S11 (A) Digital photo and **(B)** ^{1}H NMR spectrum of the as-prepared solution of Li_2S and $Zn(OAc)_2$·DEA with molar ratio of 2:1, and then add Li_2S_6 with the same amount as Li_2S in CD_3OD; **(C)** The proposed reaction between $Zn(SLi)_2$·DEA and Li_2S_6.

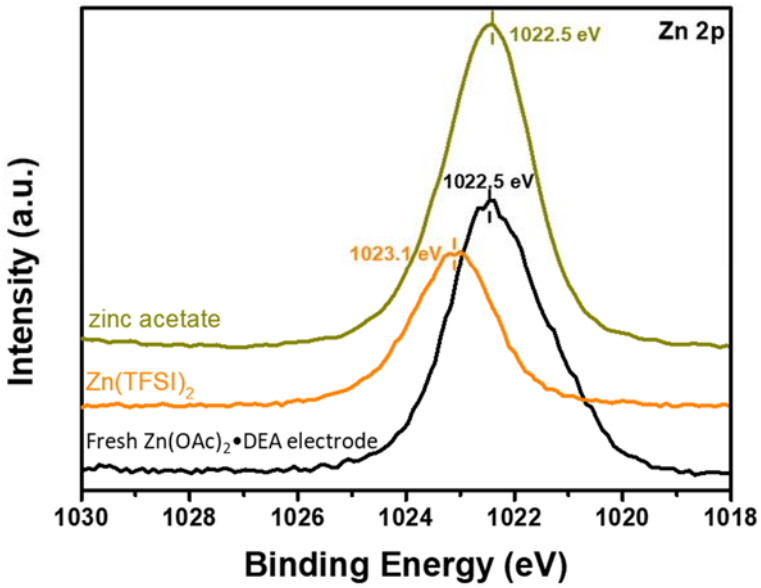

Fig. S12 Zn 2p XPS spectra of the fresh $Zn(OAc)_2 \cdot DEA$ based sulfur cathode, pure $Zn(TFSI)_2$ (zinc(II) bis(trifluoromethanesulfonyl)imide) and pure zinc acetate**.**

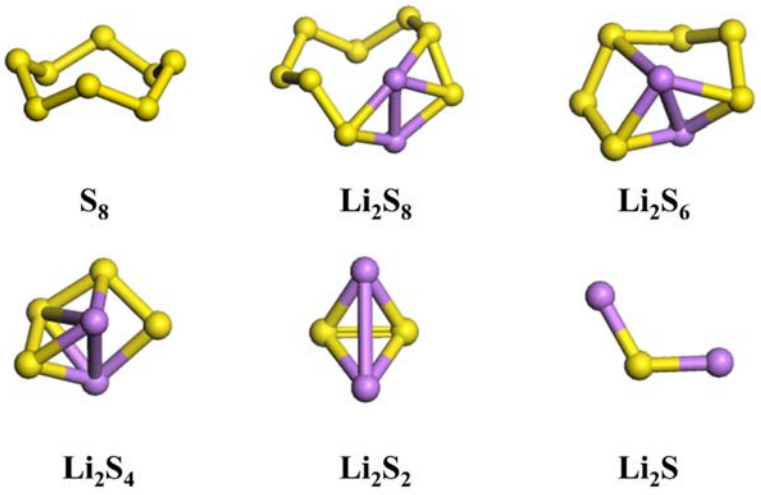

Fig. S13 The optimized geometries of S_8 and different LPS. The yellow and purple balls represent S and Li atoms, respectively.

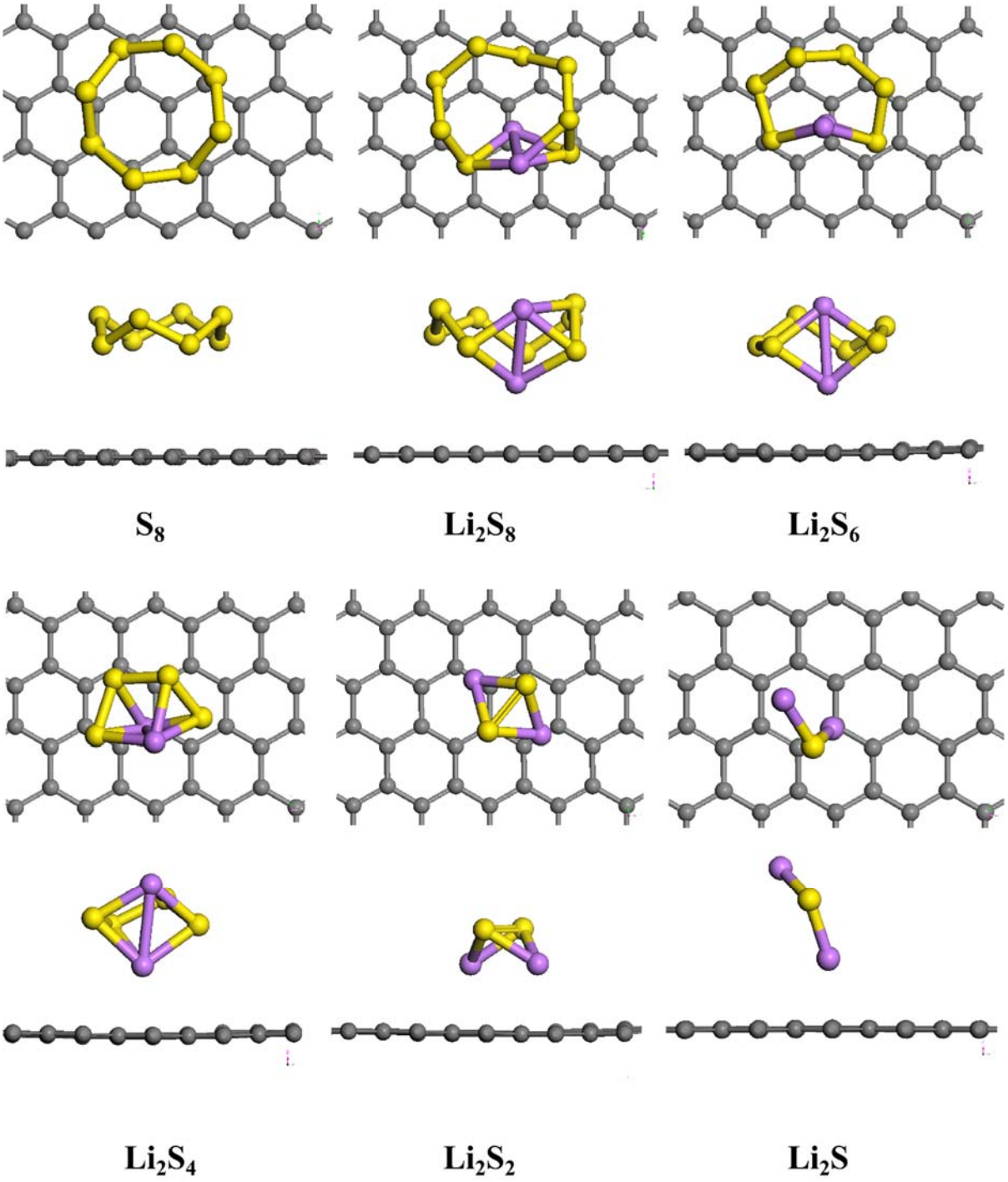

Fig. S14 The optimized adsorption conformations of S_8 and different LPS on the graphene substrate. The grey, yellow and purple balls represent C, S and Li atoms, respectively.

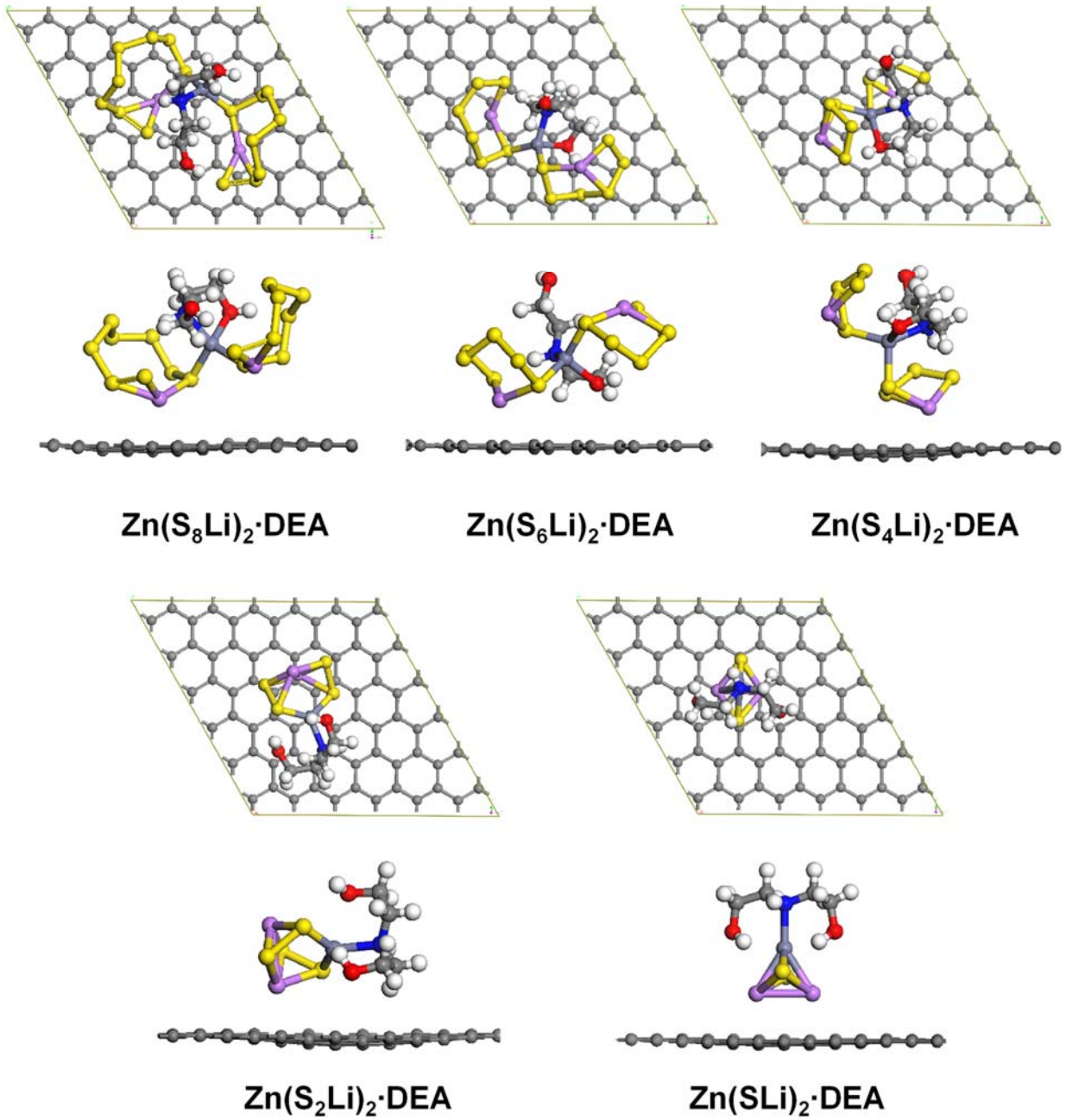

Fig. S15 The optimized adsorption conformations of the compounds of S_8, LPS and $Zn(OAc)_2$·DEA on the graphene substrate. The grey, red, white, yellow, purple, dark blue, and grey blue balls represent C, O, H, S, Li, N, and Zn atoms, respectively.

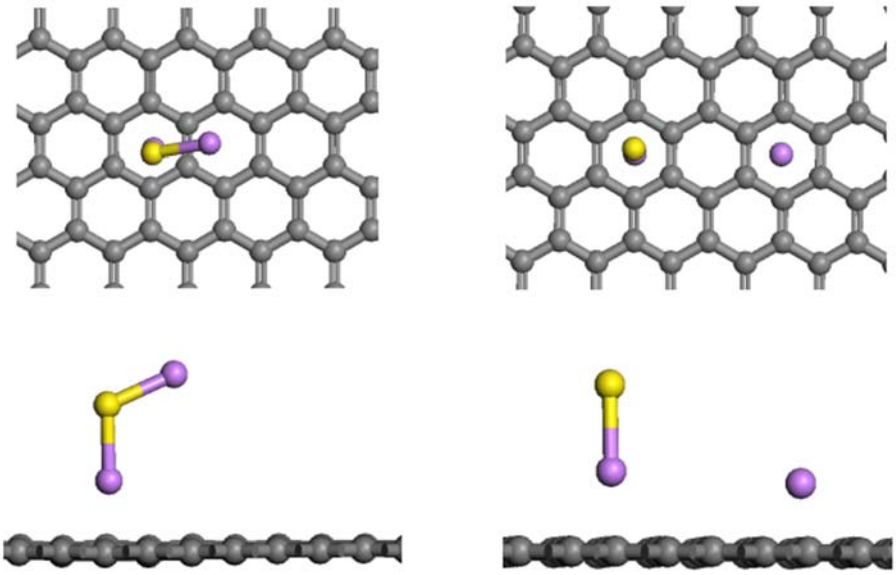

$$Li_2S \rightarrow LiS + Li$$

Fig. S16 The initial and final structures in the dissociation of Li_2S on graphene substrate. The yellow and purple balls represent S and Li atoms, respectively.

4. Supplementary Tables

Table S1. Summary of UV-vis measurement results of LPS trapping experiments.

Exp.#	Sample preparation					UV-vis data (Li_2S_6)		LPS trapping efficiencies	
	$Zn(OAc)_2 \cdot DEA$		Li_2S_6		Super P				
	$n_{Zn\text{-}DEA}$, μmol	$c_{Zn\text{-}DEA}$, mM	n_{LPS}, μmol	c_0, mM	mg	A	c, mM	η_n	η_m
1	20.8	0.520	50.0	1.25	12.0	0.04	0.346	1.74	1.24
2	7.8	0.195	37.5	0.938	4.5	0.14	0.579	1.84	1.31
Average								1.8	1.3

Table S2 Trapping capability of $Zn(OAc)_2$·DEA in comparison with selective reported LPS trappers.

LPS Trapper	LPS tested	Trapping capability		Refs.
		Mass efficiency[a] (η_m)	Molecular efficiency[b] (η_n)	
		$g_{LPS}/g_{trapper}$	$mol_{LPS}/mol_{trapper}$	
V_2O_5	Li_2S_6	0.0163	0.0142	5
MnO_2		0.124	0.0566	
V_2O_3		0.0292	0.0211	
Ti_4O_7		0.022	0.0322	
TiO_2		0.0178	0.0069	
SiO_2		0.0107	0.003	
Al_2O_3		0.0021	0.001	
TiS_2		0.0717	0.0389	
FeS		0.0087	0.00365	
MoS_2		0.035	0.0271	
Cu_2S		0.0042	0.0033	
CuS		0.0028	0.0013	
TiN		0.0083	0.0026	
ZnS		0.041	0.0195	
CoS		0.0006	0.0003	
Carbon black		0.0223	0.0012	
HC-1	Li_2S_6	0.04	0.0023	1
HC-2		0.053	0.003	
HC-3		0.047	0.0027	
HC-2-9%$_{oxygen}$		0.085	0.0049	
g-C_3N_4	Li_2S_4 (Li_2S_6)[d]	0.41 (0.59)	0.27	*6*
NdC		0.24 (~0.35)	0.26	
Meso-TiO_2		0.23 (~0.33)	0.13	
carbon microsphere (CM)	Li_2S_6	0.072	0.0042	*7*
V_2O_3 modified carbon microsphere (VCM)		0.090	-	
Polyimide (PI)	Li_2S_6	0.083	0.16[c]	*8*
$Zn(OAc)_2$·DEA	**Li_2S_6**	**1.3**	**1.8**	**This work**

a: The mass efficiencies of trappers reported in ref. 5 were calculated using the trapping capacity data in units of g_{LPS} m^{-2} trapper and the surface area (m^2 g^{-1}) of the trapper reported.

b: The molecular efficiencies (η_n) for the trappers reported in the literature were calculated using Eq. (3) using the mass efficiencies (η_m).

c: The molar mass of the repeat unit for the polyimide (structure shown below), 394.39 g mol^{-1}, was used as the M_{trap} for the calculation of the molar efficiency, η_n, using Eq. (1).

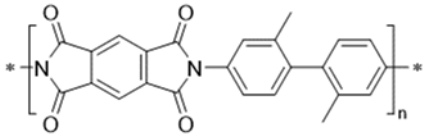

Chemical Formula: $C_{24}H_{14}N_2O_4^{2\bullet}$
Molecular Weight: 394.39
Polyimide (PI)

d: Li_2S_4 was used for the LPS trapping tests in ref.7. The mass efficiencies of the trappers in terms of Li_2S_6 were converted from the reported data based on Li_2S_4 and listed inside the brackets for comparison with other trappers.

References

1. Schneider, A., Janek, J. & Brezesinski, T. Improving the capacity of lithium-sulfur batteries by tailoring the polysulfide adsorption efficiency of hierarchical oxygen/nitrogen-functionalized carbon host materials. *Phys. Chem. Chem. Phys.* **19**, 8349-8355, (2017).
2. Wang, C. *et al.* Unravel the Catalytic Effect of Two-Dimensional Metal Sulfides on Polysulfide Conversions for Lithium-Sulfur Batteries. *ACS Appl. Mater. Inter.* **12**, 43560-43567, (2020).
3. Hayami, R. *et al.* Zinc-diethanolamine complex: synthesis, characterization, and formation mechanism of zinc oxide via thermal decomposition. *J. Sol-gel. Sci. Techn.* **87**, 743-748, (2018).
4. Novák, P. Overoxidation of polypyrrole in propylene carbonate. *J. Electrochem. Soc.* **138**, 3300, (1991).
5. Wu, D. S. *et al.* Quantitative investigation of polysulfide adsorption capability of candidate materials for Li-S batteries. *Energy Stor. Mater.* **13**, 241-246, (2018).
6. Pang, Q. & Nazar, L. F. Long-life and high-areal-capacity Li-S batteries enabled by a light-weight polar host with intrinsic polysulfide adsorption. *ACS Nano* **10**, 4111-4118, (2016).
7. Tang, R., Li, X., Ding, Z. & Zhang, L. An ultrafine V_2O_3 modified hierarchical porous carbon microsphere as a high performance cathode matrix for lithium-sulfur batteries. *RSC Adv.* **6**, 65162-65170, (2016).
8. Kim, M.-J. *et al.* Polyimide-coated glass microfiber as polysulfide perm-selective separator for high-performance lithium-sulphur batteries. *Nanomaterials* **9**, 1612, (2019).